Preprints of the 5th IFAC Symposium on Mechatronic Systems
Marriott Boston Cambridge
Cambridge, MA, USA, September 13-15, 2010

MECHATRONICS2010-117

A new sample-profile estimation signal in dynamic-mode atomic force microscopy ⋆

Chibum Lee * **Srinivasa M. Salapaka** **

* *Department of Mechanical Sciences and Engineering, University of Illinois at Urbana-Champaign, Urbana IL, 61801, USA (e-mail: clee62@illinois.edu).*
** *Department of Mechanical Sciences and Engineering, University of Illinois at Urbana-Champaign, Urbana IL, 61801, USA (e-mail: salapaka@illinois.edu).*

Abstract: In this paper, a design scheme is proposed that separates the issues of sample-profile estimation and amplitude regulation in dynamic-mode atomic force microscopy. In current AFM, the control signal for amplitude regulation is also used as the estimate for the sample-profile. Therefore, the sample profile estimation signal is accurate as long as the sample-profile signal perceived by the cantilever is well within the bandwidth of the control transfer function. In the proposed design scheme, maintaining a constant amplitude while scanning at high bandwidth does not impose limitations on the reconstruction of the sample topography. In fact, we analytically prove that the sample-profile signal estimation problem can be solved independently of the control design scheme for amplitude regulation. Therefore, accurate sample-profile estimations can be obtained even at frequencies near and beyond the closed-loop control bandwidths. However, we show that the robustness of estimation does depend on the control design for regulation and in fact, the robustness of estimation is described by the closed-loop sensitivity transfer function. The independence of the profile-estimation problem from the control design is another salient distinguishing characteristic of this work. The estimation bandwidths by this new scheme are improved significantly over commonly used signals. Comparison with the existing methods of using the control signal as the image is provided. The experimental results corroborate the theoretical development.

Keywords: High bandwidth, AFM, Robust control, Optimal control, Estimation

1. INTRODUCTION

Atomic force microscope (AFM) was invented by Binnig, Quate and Gerber (Binnig et al. (1986)), and forms one of the most versatile and widely used nano-scale microscopy that has already demonstrated atomic-scale imaging and manipulation of matter (see Figure 1).

Depending on the sample and intended applications, various imaging modes are obtained by appropriate actuation strategies. In the static mode operation, the tip scans the sample in contact with the surface. The most prevalent static mode operation is the constant force mode where the static tip deflection is used as a feedback signal. If the measured deflection is different from the set point value, the feedback controller applies a voltage signal to extract or retract the vertical piezo to keep the deflection constant. A constant cantilever deflection means that a constant force is applied to the cantilever. The control signal is usually used as a measure of the height of topographic features on the sample. The advantages of this mode are the high scan speed, the atomic resolution imaging, the ease of data interpretation and the ease of implementation.

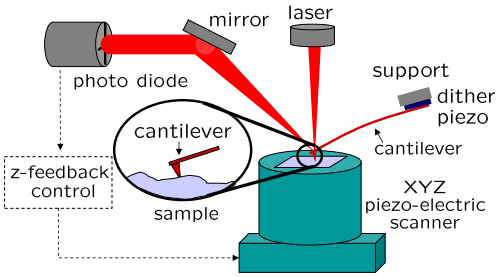

Fig. 1. Atomic force microscope: The main probe of an atomic force microscope is a microcantilever, which deflects due to interactive forces between the atoms on the sample and the atoms on the tip. The deflection of the cantilever is registered by a laser incident on the cantilever, which reflects onto a photodiode. The difference between the readings from the top and the bottom cells gives a measurement proportional to the cantilever's normal deflection. The measured deflection signal is used to design a feedback control that moves the piezo-positioner vertically in order to compensate for the effect of topographical features of the sample on the cantilever tip.

⋆ This work was supported by NSF Grant Nos. ECS 0925701 and CMMI 0800863.

In the dynamic mode operation, the cantilever is externally oscillated at frequency close to its resonance frequency or a harmonic by forcing the base that supports the cantilever with a dither piezo. The cantilever oscillations vary when it interacts with the features on the sample. Thus, the changes in amplitude, phase and frequency of the cantilever oscillations are indicative of the effects of the tip-sample interaction forces and can be used to infer sample properties (the sample topography being one of them). Dynamic mode operations where the tip oscillate in the attractive regime are called non-contact mode (Giessibl (2002)), and dynamic mode operations where the tip probes both the attractive and the repulse regime are called intermittent mode or tapping mode. The amplitude modulation AFM (AM-AFM) method with intermittent contact is the most used mode for the characterization and modification of various materials in ambient condition. One of the foremost requirements in many applications, especially in imaging of soft bio samples such as cells, tissues and proteins, is that the cantilever is gentle on the sample and does not damage the sample. These applications therefore preclude contact-mode AFM, since the cantilever can tear through the sample surface. The dynamic-mode AM-AFM is more commonly used for imaging, since they come in contact only intermittently with the sample and the cantilever does not drag through the sample.

Since the sample-topography data is interpreted from the steady state amplitude values of the deflection signal in existing methods, the imaging is slow. Another challenge for fast-imaging in AM-AFM stems from the high frequency oscillation of the cantilever which poses practical as well as analytical complications. The cantilever oscillates on the order of 100 kHz, while the scanning systems are typically two orders slower, that is the control bandwidth is in $0.1-3$ kHz range. This forms the main motivation for using slow derivative signal (such as the amplitude signal) instead of the deflection signal itself. Obtaining these derivative signals adds further complexity in the model which makes the analysis of the AM-AFM even more difficult. Although the resulting dynamics and their simplifications have been modeled and analyzed using various tools (García and Pérez (2002); Sebastian et al. (2001); Lee et al. (2003); Giessibl (2003); Sulchek et al. (2002); Gauthier et al. (2001)), the models have not been used in designing control. In current methodologies, the sample-topography is typically estimated through set-point regulation using proportional-integral-derivative (PID) feedback laws.

System theoretical approaches in force regulation and profile estimations have been researched in the past. Kodera et al. (2006); Agarwal et al. (2009) proposed a switching of PID controller in dynamic mode operation, to reduce probe-loss affected regions in an image. In Schitter et al. (2003), the feedforward controller for previous scan line, as well as the feedback controller in contact mode operation is designed in $\mathcal{H}_\infty$ robust optimal framework for having better bandwidth and robustness. Salapaka et al. (2005) used a new scheme for obtaining better imaging bandwidth, where the control signal is used only for contact-force regulation while a separate signal is derived to estimate the sample topography. It adopts $\mathcal{H}_\infty$ robust optimal control framework in the design of these signals.

This paper is organized as follows: Section 2 provides the modeling of dynamic AFM. In section 3, the new estimation signal is proposed. In section 4, the effectiveness of new signal is demonstrated on an dynamic AFM imaging and substantiated through experimental results. An analysis and discussion of the proposed methodology and its implementation are presented in section 5.

2. MODELING OF DYNAMIC AFM

To interpret the operating principle of imaging in control perspective, the block diagram schematic of an imaging in typical AFM is introduced in Figure 2, which excludes the x-y positioning system. The controller, the vertical piezo positioner, the cantilever dynamics model which includes the tip-sample interaction force, and the signal conditioner are represented by K, G_p, $\mathcal{F}$, and $\mathcal{Q}$ respectively.

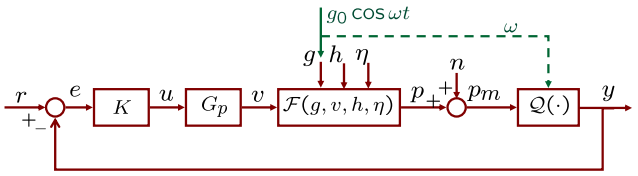

Fig. 2. A block diagram schematic of an AFM: The controller K is designed to regulate the difference e between a derivative y of the deflection signal p and the set point r to zero to compensate the effects of the sample topography h. The deflection p is due to the forcing of the nonlinear dynamic model $\mathcal{F}$, the dither piezo excitation g, the thermal noise η, and the tip-sample interaction force F_{ts} that depends on the sample-position v by vertical piezo actuator and the sample height h. The deflection measurements p_m are corrupted by sensor noise, that is, $p_m = p + n$.

The various modes of operation differ in their designs of the dither control input g, the output y derived from the the deflection signal p, and the way the feature height h is interpreted from the measurements. For instance, in contact-mode constant force microscopy, the dither is not excited ($g = 0$) and the measured deflection signal p_m is regulated at a constant ($Q(\cdot)$ is the identity operator) value by appropriately designing the control signal u. If the effects of thermal η and sensor noise n are neglected, the tip-sample interaction force, which is a function of $p - h + v$, is approximately a constant since the deflection p is regulated at a constant value, which in turn implies that topography $h = v$. Since $v = G_p u$ and G_p is approximately a constant at low frequencies, the control signal u (the input to the vertical piezoactuator) gives a measure proportional to h for low speed scans. Similarly in AM-AFM, the dither piezo is oscillated at a frequency ω close to the cantilever natural frequency ω_0, (i.e., $g(t) = g_0 \cos(\omega t)$), and the amplitude of the cantilever deflection p_m is regulated at a constant value. Again, the control signal u gives a measure of the topography h since the sample position v compensates for the effects of h to regulate the amplitude of the deflection signal. In fact, the control signal u from force regulation technique forms the topography signal in most existing imaging modes. However, this signal yields distorted (or no) images for

high speed scans (or rough samples) since G_p is not constant and u is not proportional to sample position v at high frequencies.

3. NEW ESTIMATION SIGNAL

In this study, we address fast and accurate imaging in dynamic mode operation. In AM-AFM in Figure 2, the controller K is designed to regulate the amplitude of cantilever deflection p to compensate the effects of the sample topography h. Since the controller signal u is also used as the estimate for the sample topography (obtained by multiplying the control u by multiplying pre-calibrated vertical piezo-positioner sensitivity), the controller K needs to achieve both good set-point regulation as well as good estimation of the sample topography.

The new approach proposes the use of a separate estimator K_2 to fully utilize the information in the system as seen in Figure 3(a). It is assumed that the set point regulation controller K_1 is already given or fixed. In this design, a new estimator K_2 and a sample-topography estimate signal $\hat{h}$ are introduced, where a norm on error $h-\hat{h}$ serves a metric of the accuracy of estimation.

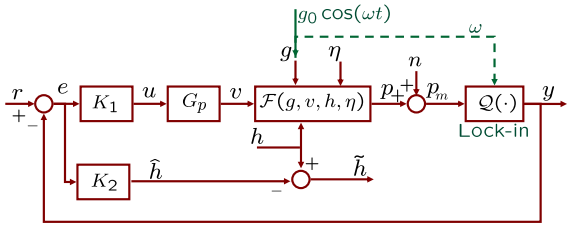

(a)

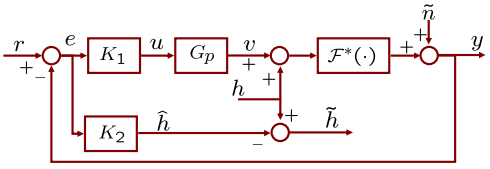

(b)

Fig. 3. Block diagram for the model-based scheme for sample-topography estimation: K_2 is a separate estimator and $\hat{h}$ is a new estimate signal. The multi-input cantilever dynamics model $\mathcal{F}(g,v,h,\eta)$ and lock-in amplifier $\mathcal{Q}(\cdot)$ in (a) is approximated by the single input model $\mathcal{F}^*(\cdot)$.

In Figure 3(b), we present a block diagram that represents a model for AM-AFM. Here $\mathcal{F}^*(\cdot)$ represents the map whose output is the amplitude of the deflection signal when its input is the sum of the sample-topography and the piezoactuation signals. This nonlinear map can be obtained using asymptotic perturbation methods to remove high frequency oscillation originating from g (Wang (1998); Sasaki and Tsukada (1999)). This model can be thought of representing the combination of the cantilever dynamics along with the lock-in amplifier in Figure 3(a). Here, $\tilde{n}$ represents the uncertainties for using $\mathcal{F}^*(\cdot)$ and the effect of the noise n. Under assumptions that the given controller K_1 and the vertical piezo model G_p are linear maps, the input u is given as $u = K_1(r-n-\mathcal{F}^*(h+G_p(u)))$. Also, we represent the nonlinear map $\mathcal{F}^*$ as linear transfer function with multiplicative uncertainty $\mathcal{F}^* = F(1+w_i\Delta)$ as in Figure 4, where the stable weight transfer function w_i reflects frequency dependence on uncertainty. Based on our identification experiments, the cantilever dynamics is nearly linear at low frequencies ($\leq$ 2 kHz and hence the weight w_i can be chosen to be small at this frequency range. In this framework, input u can be written as

$$u = \begin{bmatrix} SK_1 & -SK_1F \end{bmatrix} \begin{bmatrix} r-\tilde{n} \\ h \end{bmatrix} \tag{1}$$

where $S = (1 + K_1FG_p)^{-1}$ represents the sensitivity function. In conventional estimation, the transfer function

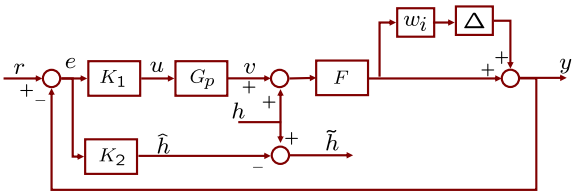

Fig. 4. Block diagram with multiplicative model uncertainty: $\mathcal{F}^* = F(1 + w_i\Delta)$ with any stable function with $\|\Delta\| < 1$.

from the sample profile h to the control signal u is given by $SK_1F = K_1F/(1 + G_pK_1F)$. For achieving amplitude regulation, K_1 is required to be high at low frequencies, which implies that the transfer function from topography h to the control u can be approximated by $1/G_p$ at low frequencies. Since the frequency response of the piezoactuator is approximately a constant at low frequencies (upto its bandwidth), $|G_p(0)|u$ is used as an estimate of the sample topography h. However, at high frequencies, K_1 can not be designed to be large as it can make the closed-loop unstable especially in the view of modeling uncertainties $w_i\Delta$. In amplitude modulation dynamic mode, the large K_1 typically induces a *chatter-phenomenon* in imaging even though it does not make system unstable. As a result, the transfer function from the topography signal to the control signal u is not a constant. Therefore, this control signal (that is, the input to the piezo actuator), which is typically used as an estimate for sample topography, gives low fidelity images during fast scanning. Note that the temporal frequency content of h depends on the spatial frequency content of the sample, i.e. how rough the sample is, and the scanning rate of the lateral positioners, i.e. how fast the sample is scanned. Thus, easy solution for good imaging is to use a slow lateral scanning rate which will make h the low frequency signal with moderate K_1 controller. However, this solution comes by sacrificing bandwidth, which is not tenable in many applications.

Now we analyze the proposed signal $\hat{h}$ for sample-topography estimation (see Figure 4). The estimate signal $\hat{h}$ can be written as

$$\hat{h} = \begin{bmatrix} K_2S & -K_2FS \end{bmatrix} \begin{bmatrix} r-\tilde{n} \\ h \end{bmatrix} \tag{2}$$

where the sensitivity transfer function S depends only on K_1 and not on K_2. An estimate $\hat{h}$ can be obtained by designing $K_2 = -S^{-1}F^{-1}$ since it minimizes the estimation error $\tilde{h}$ from h given by

$$\tilde{h} = [\,-K_2S \quad 1 + K_2FS\,] \begin{bmatrix} r - \tilde{n} \\ h \end{bmatrix}. \tag{3}$$

Note that S is invertible since it is bi-proper and has no non-minimum zero when K and G are stable, which is typically true. If F is strictly proper, low pass filter weight function W of the order equal to the relative degree of F can be used to make $K_2 = -S^{-1}F^{-1}W$. If F has a non-minimum zero, then K_2 can be obtained through a Nevanlinna-Pick solution to a model-matching problem $arg\min_{/k_2} \|K_2FS+1\|$ (e.g. see Lee and Salapaka (2009)).

One important consequence of this design is that it decouples the objectives of regulation and sample-topography estimation. The design of controller K_1 for regulation can be made without any consideration towards estimation of sample topography. In this design, the estimation bandwidth is not limited by the regulation bandwidth. Another advantage of this separation of designs is that the improvement in the estimation bandwidth is achieved without increasing the range of frequencies where control $|K_1|$ has high values, which means that it avoids the the stability or chattering issues discussed earlier.

Equation (3) clearly shows the trade-off between image estimation bandwidth and noise attenuation. If we design $K_2 = -S^{-1}F^{-1} = (1 + K_1FG_p)F^{-1}$ to achieve high estimation bandwidth, then the estimate signal $\hat{h}$ will be corrupted by the effect of noise $K_2S\tilde{n} = F^{-1}\tilde{n}$. Thus, augmenting the estimator with a weight function W_h that carries the information content of height signal h results in

$$K_2 = -S^{-1}F^{-1}W_h \tag{4}$$

and the corresponding estimation error is given by $\tilde{h} = -F^{-1}W_h(r - \tilde{n}) + (1 - W_h)h$. f we choose the weight function W_h low pass filter, the effect of noise $F^{-1}W_h\tilde{n}$ rolls off at high frequencies.

In summary, new method separates the goals of force regulation and sample-topography estimation by designing two signals - u for force regulation and $\hat{h}$ for estimating the sample topography h. The control signal bandwidth is limited due to practical requirements such as stability and robustness to modeling uncertainties. Therefore, the control signal serves as a poor estimate of sample topography near and beyond the control-bandwidth frequency. The separation of goals allows the estimation signal $\hat{h}$ to depend directly on the whole frequency range of the amplitude signal (both below and beyond the control-bandwidth, thus more sample-topography information) and give accurate estimates of the sample topography.

4. EXPERIMENTAL SETUP AND RESULTS

4.1 Device description

We demonstrated this design for sample-topography estimation on MFP-3D, an AFM developed by Asylum Research Inc. A schematic of this device is shown in Figure 5.

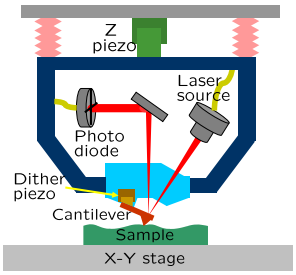

Fig. 5. A schematic of imaging system of MFP-3D.

The voltage range of vertical piezo is -10 to 150 V and travel range is 25 μm. The cantilever deflection p is sampled at 5 MHz with 16 bit resolution for amplitude and phase calculations using a lock-in amplifier that is built on Field Programmable Gate Array (FPGA) and Digital Signal Processor (DSP). Amplitude signal is down-sampled to 100 kHz. The controller K_1 and the estimator K_2 which run at 100 kHz are implemented on DSP. This DSP code takes the amplitude signal and the set point value as input and generates the control effort, which is converted by 20 bit 100 kHz DAC and applied with the vertical piezo after amplification.

The cantilever used for the experiment is AC240TS by Olympus co., which is approximately 240 μm long, 30 μm wide and its tip is approximately $<$ 10 nm in diameter. The nominal value of resonant frequency is 70 kHz.

Most commercial AFMs offer the proportional-integral (PI) or proportional-integral-integral (PII) controllers as a default controller. The controller K_1 needs to be decided depending on the cantilever used since it determines the dynamics $\mathcal{F}(g, v, h, \eta)$ for the same system with the vertical piezoactuator G_p and the lock-in amplifier Q. The controller K_1 is tuned as $K_1(s) = -\frac{6000}{s}$, which did not induce the chattering and gave a good quality image at slow scan.

4.2 Vertical piezo identification

Since physical modeling of the device is difficult, identification techniques were used to derive the transfer function from the vertical-piezo input u to the reading of z-position sensor. At various points in the operating range, we obtained the frequency response of the vertical piezo over $0-10$ kHz (Figure 6(a)). The nominal frequency response of the device was chosen, at which the amplitude modulation would be set. Figure 6(b) shows the bode diagram of fitted mathematical model with nominal experimental result. Weighted iterative least square fitting was performed over $0 - 7.5$ kHz and resulted in following model:

$$\begin{aligned} G_z(s) = {} & \frac{-2.3808 \times 10^7 (s - 2.244 \times 10^4)}{(s + 5.455 \times 10^4)(s^2 + 523.4s + 1.164 \times 10^8)} \\ & \times \frac{(s^2 + 352.1s + 1.212 \times 10^8)(s^2 + 3961s + 2.079 \times 10^8)}{(s^2 + 7252s + 1.893 \times 10^8)(s^2 + 1056s + 1.993 \times 10^8)} \\ & \times \frac{(s^2 + 257.3s + 2.595 \times 10^8)(s^2 - 73.47s + 5.126 \times 10^8)}{(s^2 + 240.9s + 2.637 \times 10^8)(s^2 + 1163s + 5.119 \times 10^8)} \\ & \times \frac{(s^2 - 2020s + 1.157 \times 10^9)(s^2 + 546s + 1.536 \times 10^9)}{(s^2 + 509.7s + 1.326 \times 10^9)(s^2 + 3090s + 1.678 \times 10^9)} \\ & \times \frac{(s^2 + 701.9s + 2.183 \times 10^9)}{(s^2 + 2643s + 2.136 \times 10^9)}. \end{aligned} \tag{5}$$

The z-position sensor has the sensitivity of 1.3×10^{-6} m/V. The transfer function between the vertical-piezo input u to its displacement v is given by $G_p(s) = 1.3\times10^{-6}\ G_z(s)$.

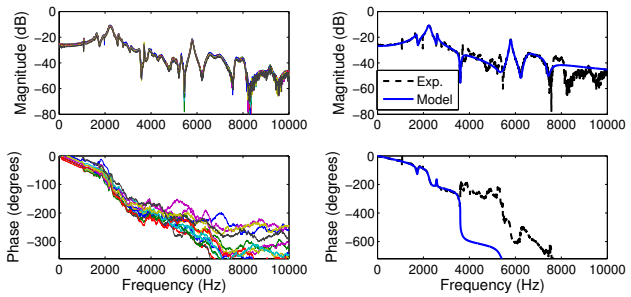

(a) (b)

Fig. 6. Identification of vertical piezo: (a) Experimental frequency responses at various operating positions (b) Nominal frequency response(dashed) and model frequency response(solid).

4.3 Estimator design

The cantilever dynamics model $\mathcal{F}^*$ is assumed as the Krylov-Bogoliubov-Mitropolsky(KBM) approximation with assumption of the sample height h and the vertical piezo position v being constant while one period of oscillation. In the derived KBM model, the error depends on the order of ϵ expansion, decays to zero in steady state, and it has good fidelity in slow varying inputs, where the decay is faster than the input changes, but not in fast varying inputs. In the frequency range up to ω_i mentioned in previous section, the cantilever dynamics F is linear (in fact, it is almost constant), and at the frequencies above ω_i, the non-linear dynamics can be considered as the uncertainty Δ. For these reasons, F was chosen as the dc gain of the KBM approximation ($F = -0.998 \approx -1$). W_h chosen as the low pass filter with 2 kHz bandwidth, $W_h = \frac{1}{7.958\times10^{-5}s+1}$. Since the output of F is the amplitude of the displacement and required to converted to the voltage signal, F used in in the estimator design is scaled by the optical lever sensitivity, 359.7×10^{-9} m/V, which depends on each attachment of cantilever.

The resulting estimator K_2 is obtained and the balanced model reduction results in the following 6th order model:

$$K_2 = \frac{5.4639(s+4.639\times10^5)(s+1211)(s^2+1357s+1.186\times10^8)}{(s+0.001)(s+6609)(s^2+1109s+1.2\times10^8)} \times \frac{(s^2+2554s+1.84\times10^8)}{(s^2+2116s+1.96\times10^8)}. \quad (6)$$

To validate this new estimation method, several samples are imaged. Every experiment was performed in raster scan with various scanning rate. The conventional height estimate $\hat{u}$ and the new height estimate $\hat{h}$ was obtained simultaneously while scanning.

4.4 1D imaging results

The calibration grating TDG01 from NT-MDT co. was imaged. It has 1 dimensional parallel ridge pattern with the height of approximately 50 nm and the period of 278 nm (3600 lines/mm). The structure was formed on the glass wafer. Figure 7 shows slow scan (4 μm/sec) image constructed from the conventional estimate signal $\hat{u}$.

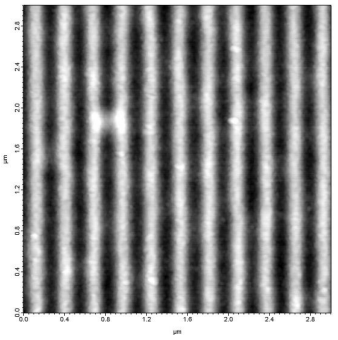

Fig. 7. Slow scan (4 μm/sec) image of TDG01 constructed from the conventional estimate signal $\hat{u}$.

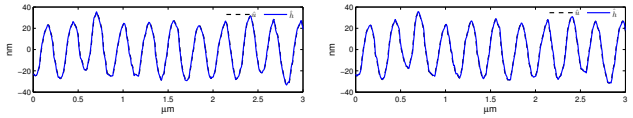

(a) (b)

Fig. 8. The conventional estimate signal $\hat{u}$(dashed) and the new estimate signal $\hat{h}$(solid) of slow scan of TDG01: (a) trace (left to right) direction (b)retrace (right to left) direction

The conventional estimate signal $\hat{u}$ and the new estimate signal $\hat{h}$ of slow scan (4 μm/sec) are compared in trace (left to right) direction in Figure 8(a) and in retrace (right to left) direction in Figure 8(b). Since the two signals are almost identical in both trace and retrace, which is natural because the X-Y positioner operated in feedback loop does not have the hysteresis effect Sebastian and Salapaka (2005), the average of these four signals is considered as the real feature and used as a reference for the calculation of error in fast scan. The deviations from the reference are 2.3013 nm ($\hat{u}$-reference in trace direction), 1.6855 nm ($\hat{u}$-reference in retrace direction), 1.1104 nm ($\hat{h}$-reference in trace direction), and 0.7641 nm ($\hat{h}$-reference in retrace direction) in root mean square (RMS) value.

Figure 9 compares the conventional estimate signal $\hat{u}$ and the new estimate signal $\hat{h}$ of trace scan lines in left column, and the error of conventional estimate $\hat{u}$ − reference and the error of the new estimate $\hat{h}$ − reference in right column. Since the calibration grating TDG01 is manufactured for X-Y positioner calibration, its spacial pitch of 278 nm is quite accurate. Thus, we can calculate the temporal excitation frequency from this pitch and the scan velocity, thus a scan velocity of 10 μm/sec (shown in the scan in (a,b)) corresponds to a temporal sinusoidal frequency 36 Hz, and similarly 20 μm/sec (scan in (c,d)) to 72 Hz ,40 μm/sec (scan in (e,f)) to 144 Hz, 60 μm/sec scan in (g,h) to 216 Hz, and 80 μm/sec (scan in (i,j)) to 284 Hz. In addition to these scan velocities, the scan rates of 110 μm/sec (396 Hz), 140 μm/sec (504 Hz), and 180 μm/sec (647 Hz) were also used.

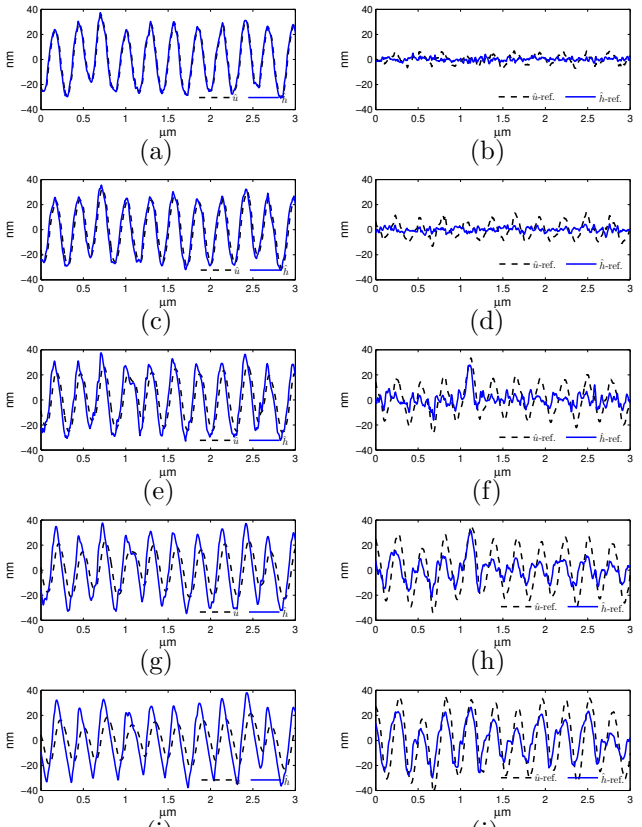

Fig. 9. Comparison of the conventional $\hat{u}$(dashed) and new estimate signal $\hat{h}$(solid): The left graphs(a,c,e,g,i) compare $\hat{u}$(dashed) and the $\hat{h}$(solid). The right graphs(b,d,f,h,j) compare $\hat{u}$-reference(dashed) and $\hat{h}$-reference(solid). (a,b) scan rate of 10 μm/sec (c,d) scan rate of 20 μm/sec (e,f) scan rate of 40 μm/sec (g,h) scan rate of 60 μm/sec (i,j) scan rate of 80 μm/sec.

Using Fourier transform on the above *input* sinsuoid time signals, the transfer function from the sample height h to the conventional height estimate $\hat{u}$ and to the the new height estimate $\hat{h}$ is obtained as shown in Figure 10(a). Figure 10(b) shows the transfer function from the sample height h to the conventional estimation error reference $-\hat{u}$ and to the the new height estimate reference $-\hat{h}$. The bandwidth of conventional estimation is approximately 177 Hz and the new estimation approximately 301 Hz.

In Figure 10(b), low magnitude values ($< -40dB$) at low frequencies is not accurate since -40 dB corresponds to the 1% of the amplitude, which is around 0.25 nm and close the resolution limit of the intermittent mode in the machine. In addition, it assumed that the input is same as the calculated reference which has the maximum RMS error of 2.3 nm, which corresponds to -21 dB. At even higher frequencies, the approximation errors due to linearization dominate (as seen in Figure ((e,f), the input-output response is not exactly linear).

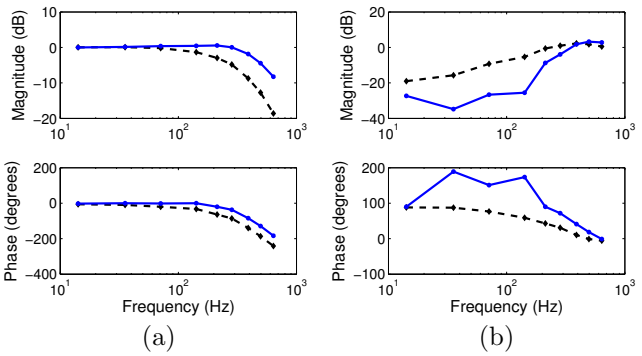

Fig. 10. Experimentally obtained transfer function of conventional(dashed) and new(solid) estimation: (a) transfer function from the sample height h to the conventional height estimate $\hat{u}$(dashed) and to the the new height estimate $\hat{h}$(solid) (b) transfer function from the sample height h to the conventional estimation error $h - \hat{u}$(dashed) and to the the new height estimate $\tilde{h}$(solid).

5. ANALYSIS AND DISCUSSION

5.1 Robustness of the new estimation

The transfer function $G_{\hat{h}h}$ from h to $\hat{h}$ is given as

$$G_{\hat{h}h} = -\frac{K_2 F}{1 + K_1 F G_p} \tag{7}$$

from (2) if we assume all transfer functions are linear.

The main source of the uncertainty in the dynamic model used in the estimation scheme is the cantilever model $\mathcal{F}_l^*$. The robustness of the new estimation signal $\hat{h}$ to the model $\mathcal{F}_l^*$ can be measured by the sensitivity of $G_{\hat{h}h}$ to the changes in the model $\mathcal{F}_l^*$. It is given by

$$\frac{dG_{\hat{h}h}}{G_{\hat{h}h}} = \frac{1}{1 + K_1 F G_p} \frac{dF}{F} = S \frac{dF}{F}. \tag{8}$$

and the robustness of the conventional estimation $\hat{u}$ to the model uncertainty $\frac{dG_{\hat{u}h}}{G_{\hat{u}h}}$ is the same. Thus, the conventional estimation method and the new estimation method has the same robustness to the cantilever model uncertainty.

5.2 Comparison with previous studies

Some estimation methods that do not directly use the controller u or the measured piezo displacement v have been proposed earlier. The *contact error mode* can be considered as intermediate between the mode of constant force mode and constant height mode (Sergei N. Magonov (1996)). This mode recognizes the fact that the control regulation bandwidth is limited and the error of regulation e has more information in Figure 3. Based on the assumption that the error e contains the sample topography information beyond control bandwidth, the sample topography estimation is obtained by summation of the scaled control u and error e signals, that is, estimate signal $\hat{h}$ is obtained as $\hat{h} = \alpha u + \beta e$, where α and β are constants. The main disadvantages of these mode are: 1) the prescription of α and β is ad-hoc and typically these estimates do not result

in significant improvement of the imaging bandwidth. The primary reason is that these scaling factors need to be dynamic as reflected in our design.; and 2) unlike our design, this design does not consider robustness to the noise and the disturbance signals. The effects of the noise is clearly seen from the equation for the estimate signal given by there are no consideration on the noise and disturbance signal. The error signal e is contaminated by the effect of the noise and disturbance, especially in dynamic mode operation in atmosphere. The estimate used in this mode can be given in

$$\hat{h} = (\alpha K_1 + \beta)S(r - \tilde{n}) - (\alpha + \beta K_1)S\mathcal{F}_l^*(h). \quad (9)$$

The proposed design can be viewed as a generalization of the method described in Salapaka et al. (2005) for contact mode AFM. Contact mode AFM lends to simpler linear analysis for the following two reasons: since the tip-sample interaction is always regulated in the the repulsive region, the tip-sample interaction force $F_{ts}(p - h - v)$ is well modeled by the linear relationship $F_{ts}(p-h-v) = k_o(p-h-v)$ for some constant k_o; and also, the cantilever transfer function is assumed a constant G_c, which is a good approximation since micro-cantilevers have much larger bandwidths than the vertical positioning systems. In the research, the controller K_1 is designed by stacked sensitivity synthesis and the estimator K_2 design utilized the state estimator aspect of $\mathcal{H}_\infty$ solution of the controller K_1. However, this model based research has the same issue of model uncertainty in dynamic-mode.

5.3 Modeling uncertainty

The cantilever dynamics model $\mathcal{F}^*$ in this study is not accurate The controller K_1 is chosen heuristically not by model based methods also for the same reason.

The static model F is the most extreme case and does not reflect the real cantilever dynamics $\mathcal{F}(g, v, h, \eta)$. In dynamic mode operation, $\mathcal{F}(g, v, h, \eta)$ also include the lock-in amplifier or the rms-to-dc converter that is nonlinear and the time lag component.

As shown in Figure 10, the experimentally obtained results have smaller bandwidth than the low frequency filter W_h used. If we consider one of the uncertainty in the model, the low pass filter used in the lock-in amplifier of the given AFM, the transfer function will change as the following Figure 11.

In MFP-3D, the low pass filter (LFT) used in the lock in amplifier, is elliptic type that has large delay. In the sense that the low pass filter is considered as the separate cascade block to F, this model is not accurate as well. (In real, it is integrated in lock-in amplifier.) However, this low pass filter with cutoff frequency of 10 kHz decreases the bandwidth of imaging to 158 Hz in the conventional method and 761 Hz in the new method. The slowness and delay in lock-in amplifier or rms-to-dc converter for calculating the amplitude has been the issue in dynamic mode. The research in Ando et al. (2001) addressed this problem and used peak picking circuit for amplitude detection.

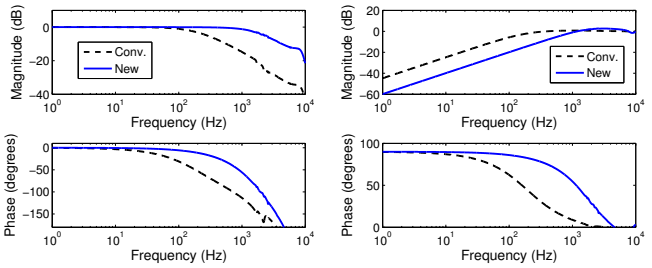

(a) (b)

Fig. 11. Transfer function of conventional(dashed) and new(solid) estimation with delay: (a) transfer function from the sample height h to the conventional height estimate $\hat{u}$ (i.e. $-SK_1\mathcal{F}_l^*LPF(s)\times$ (Piezo Sensitivity))(dashed) and to the the new height estimate $\hat{h}$ (i.e. $K_2\mathcal{F}_l^*LPF(s)S$)(solid) (b) transfer function from the sample height h to the conventional estimation error $h-\hat{u}$(dashed) and to the the new height estimate $\tilde{h}$(solid).

5.4 Best sample-topography estimate for a given feedback control

The main contribution of this paper is a design scheme that separates the regulation and the sample-topography estimation. Since design of K_1 does not depend on the design of K_2 (as is clear from the block diagram in Figure 4), the regulation as well as disturbance rejection objectives can be achieved through an appropriate design of K_1 without giving any regard for the estimation objective. Also note that, for any linear design scheme, our design of K_2 achieves the maximum estimation bandwidth (through our model matching formulation) for a *given* controller K_1. Thus improvements in the design of K_1 for larger disturbance rejection bandwidths (better robustness) will lead to larger (and the maximum possible bandwidths through linear designs) estimation bandwidth. For designing K_1, PID-based methods are most commonly used. Therefore, it may be expected that better bandwidths (for disturbance rejection) can be obtained by using robust control theoretic tools. Our recent efforts using $\mathcal{H}_\infty$ synthesis design methods did give about 20% improvement in the bandwidth over the PID designs (exhaustively searched over the parameter space); however these improvements are restricted since the linearization errors are large which limit the disturbance-rejection bandwidth of any linear robust control design. Still larger improvements in the rejection bandwidths may require nonlinear control designs and better identification of the interaction term $\mathcal{F}(g, v, h, \eta)$. However, our scheme, which separates the objectives of disturbance rejection and sample-topography estimation, will still give large improvements in sample-estimation bandwidths for a given design K_1 for the disturbance rejection. In addition, since the estimator K_2 is not in the feedback loop, it can be used either in real-time or post-processing modes.

REFERENCES

Agarwal, P., De, T., and Salapaka, M.V. (2009). Real time reduction of probe-loss using switching gain controller

for high speed atomic force microscopy. *Review of Scientific Instruments*, 80(10), 103701.

Ando, T., Kodera, N., Takai, E., Maruyama, D., Saito, K., and Toda, A. (2001). A high-speed atomic force microscope for studying biological macromolecules. *Proceedings of the National Academy of Sciences of the United States of America*, 98(22), 12468–12472.

Binnig, G., Quate, C.F., and Gerber, C. (1986). Atomic force microscope. *Physical Review Letters*, 56(9), 930–933.

García, R. and Pérez, R. (2002). Dynamic atomic force microscopy methods. *Surf. Sci. Rep.*, 47, 197.

Gauthier, M., Sasaki, N., and Tsukada, M. (2001). Dynamics of the cantilever in noncontact dynamic force microscopy: The steady-state approximation and beyond. *Phy. Rev. B.*, 64(8), 085409.

Giessibl, F. (2003). Advances in atomic force microscopy. *Reviews of Modern Physics*, 75, 949–983.

Giessibl, F.J. (2002). *Noncontact Atomic Force Microscopy*, chapter Principle of NC-AFM, 11. NanoScience and Technology. Springer, Berlin.

Kodera, N., Sakashita, M., and Ando, T. (2006). Dynamic proportional-integral-differential controller for high-speed atomic force microscopy. *Review of Scientific Instruments*, 77(8), 083704.

Lee, C. and Salapaka, S.M. (2009). Robust broadband nanopositioning: fundamental trade-offs, analysis, and design in a two-degree-of-freedom control framework. *Nanotechnology*, 20(3), 035501–035516.

Lee, S.I., Howell, S.W., Raman, A., and Reifenberger, R. (2003). Nonlinear dynamic perspectives on dynamic force microscopy. *Ultramicroscopy*, 97(1-4), 185 – 198. Proceedings of the Fourth International Conference on Scanning Probe Microscopy, Sensors and Nanostructures.

Salapaka, S., De, T., and Sebastian, A. (2005). A robust control based solution to the sample-profile estimation problem in fast atomic force microscopy. *International Journal of Robust and Nonlinear Control*, 15, 821–837.

Sasaki, N. and Tsukada, M. (1999). Theory for the effect of the tip-surface interaction potential on atomic resolution in forced vibration system of noncontact AFM. *Applied Surface Science*, 140(3-4), 339–343.

Schitter, G., Stemmer, A., and Allgower, F. (2003). Robust 2 dof-control of a piezoelectric tube scanner for high speed atomic force microscopy. *Proceeding of the American Control Conference, Denver, CO*, 3720–3725.

Sebastian, A., Salapaka, M.V., Chen, D., and Cleveland, J.P. (2001). Harmonic and power balance tools for tapping-mode atomic force microscope. *Journal of Applied Physics*, 89 (11), 6473–6480.

Sebastian, A. and Salapaka, S. (2005). Design methodologies for robust nano-positioning. *IEEE Transactions on Control Systems Technology*, 13(6), 868–876.

Sergei N. Magonov, M.H.W. (1996). *Surface Analysis with STM and AFM: Experimental and Theoretical Aspects of Image Analysis*. Weinheim, New York.

Sulchek, T., Yaralioglu, G.G., Quate, C.F., and Minne, S.C. (2002). Characterization and optimization of scan speed for tapping-mode atomic force microscopy. *Review of Scientific Instruments*, 73, 2928–2936.

Wang, L. (1998). Analytical descriptions of the tapping-mode atomic force microscopy response. *Applied Physics Letters*, 73(25), 3781–3783.